iScience

CellPress
OPEN ACCESS

Article

MBNL2 promotes aging-related cardiac fibrosis via inhibited SUMOylation of Krüppel-like factor4

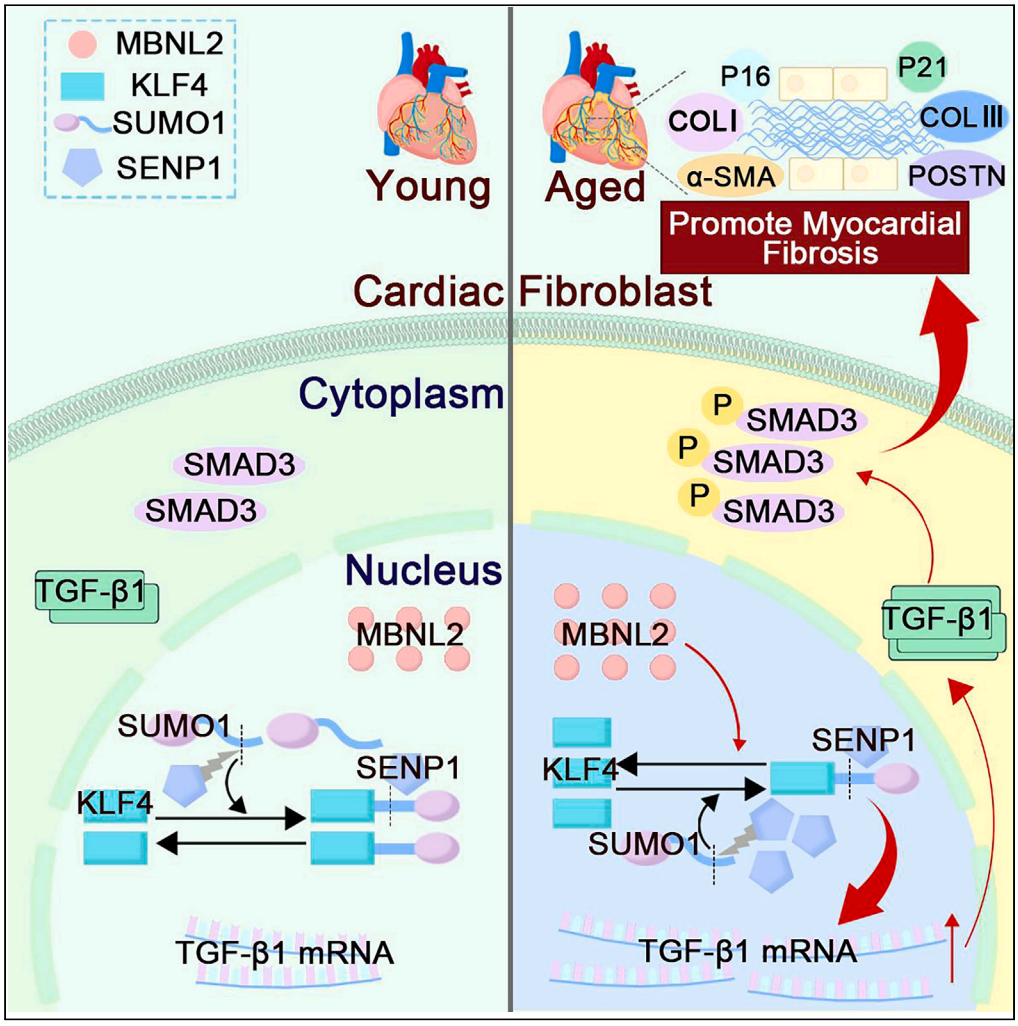

Jing Lu, Qi Zhao, Lu Wang, ..., Yuanqi Shi, Yuanyuan Guo, Zengxiang Dong

kean1943@126.com (Y.S.)
guoyuanyuan@hrbmu.edu.cn (Y.G.)
dongzx@hrbmu.edu.cn (Z.D.)

Highlights

MBNL2 promotes senescence of cardiac fibroblasts as a novel regulator

MBNL2 inhibits SUMO1 binding with KLF4

MBNL2 regulates TGF-β1/SMAD3 pathway to playing the profibrotic function

Lu et al., iScience 27, 110163
July 19, 2024
https://doi.org/10.1016/j.isci.2024.110163

iScience

CellPress
OPEN ACCESS

Article

MBNL2 promotes aging-related cardiac fibrosis via inhibited SUMOylation of Krüppel-like factor4

Jing Lu,[1,2,8] Qi Zhao,[1,2,8] Lu Wang,[2,8] Jiahao Li,[1,2] Hongyan Wang,[1,2] Lin Lv,[1,2,3] Meng Yuan,[1,2] Qiuyu Chen,[2] Zixin Zhang,[6] Dankun Luo,[7] Siqi Sheng,[2] Keying Yuan,[1,2] Guannan Liu,[1,2] Mingyu Liu,[2] Yuanqi Shi,[2,*] Yuanyuan Guo,[2,5,*] and Zengxiang Dong[2,4,9,*]

SUMMARY

Aging-related cardiac fibrosis represents the principal pathological progression in cardiovascular aging. The Muscleblind-like splicing regulator 2 (MBNL2) has been unequivocally established as being associated with cardiovascular diseases. Nevertheless, its role in aging-related cardiac fibrosis remains unexplored. This investigation revealed an elevation of MBNL2 levels in the aged heart and senescent cardiac fibroblasts. Notably, the inhibition of MBNL2 demonstrated a capacity to mitigate H_2O_2-induced myofibroblast transformation and aging-related cardiac fibrosis. Further mechanistic exploration unveiled that aging heightened the expression of SENP1 and impeded the SUMO1 binding with KLF4, and SUMOylation of KLF4 effectively increased by the inhibition of MBNL2. Additionally, the inhibition of TGF-β1/SMAD3 signaling attenuated the impact of over-expression of MBNL2 in inducing senescence and cardiac fibrosis. MBNL2, by orchestrating SUMOylation of KLF4, upregulating the TGF-β1/SMAD3 signaling pathway, emerges as a significant promoter of aging-related cardiac fibrosis. This discovery identifies a novel regulatory target for managing aging-related cardiac fibrosis.

INTRODUCTION

Aging is a multifactorial and complex process that has been associated with inflammatory and fibrotic responses, defined as a degenerative disorder affecting intrinsic physiological functions.[1] The persistent presence of senescent cells within a tissue will aggravate fibrosis development and organ dysfunction.[2,3] Consequently, a comprehensive investigation into the mechanisms governing aging-related cardiac fibrosis becomes imperative.

Muscleblind-like (MBNL) protein family, comprising MBNL1, MBNL2, and MBNL3, constitutes a protein intricately involved in the regulation of tissue-specific alternative splicing, this protein family also governs the subcellular localization and stability of mRNAs.[4–6] Notably, Cai et al. discovered that MBNL2 knockdown exhibits inhibitory effects on DNA damage repair and DNA damage-induced senescence.[7] Recent findings indicate a significant upregulation of the MBNL2 gene in patients with dilated cardiomyopathy (DCM), despite the established abnormal levels of MBNL2 in patients with DCM through clinical samples, a comprehensive investigation into the specific mechanisms underlying its impact on heart function remains imperative.[8]

KLF transcription factor 4 (KLF4) stands as a conserved transcription factor containing zinc fingers, overseeing diverse cellular processes including cell growth, proliferation, and differentiation.[9] The dynamic post-translational modification (PTM) of SUMOylation regulates various aspects of protein function, including subcellular localization, stability, conformation, transcription, and enzymatic activity.[10,11] Small ubiquitin-related modifier 1 (SUMO1) interacts with KLF4, activating transcription and impeding cell proliferation.[12] There is a research shows that SUMOylated KLF4 plays an important role in cell proliferation. The non-SUMOylated KLF4 activated P21 transcription, leading to cell growth arrest.[13] Meanwhile, SUMOylation is subject to reversal by a family of SUMO-specific proteases (SENPs). Among these, SENP1 has been identified as a specific protease responsible for the deSUMOylation of KLF4, thereby regulating KLF4 activity.[14] Our research found that SUMO1 and SENP1 dynamic regulated KLF4 in cardiac fibroblasts senescence, at the same time, MBNL2 played a crucial role in the regulated

[1]Department of Pharmacy, The First Affiliated Hospital of Harbin Medical University, Youzheng Street, Nangang District, Harbin 150001, China
[2]The Key Laboratory of Cardiovascular Disease Acousto-Optic Electromagnetic Diagnosis and Treatment in Heilongjiang Province, The First Affiliated Hospital of Harbin Medical University, Youzheng Street, Nangang District, Harbin150001, China
[3]Experimental Animal Center, The First Affiliated Hospital of Harbin Medical University, Youzheng Street, Nangang District, Harbin 150001, China
[4]NHC Key Laboratory of Cell Transplantation, The First Affiliated Hospital of Harbin Medical University, Youzheng Street, Nangang District, Harbin 150001, China
[5]Department of Cardiology, Department of Geriatrics, The First Affiliated Hospital of Harbin Medical University, Youzheng Street, Nangang District, Harbin 150001, China
[6]College of Bioinformatics Science and Technology, Harbin Medical University, Health Care Road, Nangang District, Harbin 150081, China
[7]Department of General Surgery, The First Affiliated Hospital of Harbin Medical University, Youzheng Street, Nangang District, Harbin 150001, China
[8]These authors contributed equally
[9]Lead contact
*Correspondence: kean1943@126.com (Y.S.), guoyuanyuan@hrbmu.edu.cn (Y.G.), dongzx@hrbmu.edu.cn (Z.D.)
https://doi.org/10.1016/j.isci.2024.110163

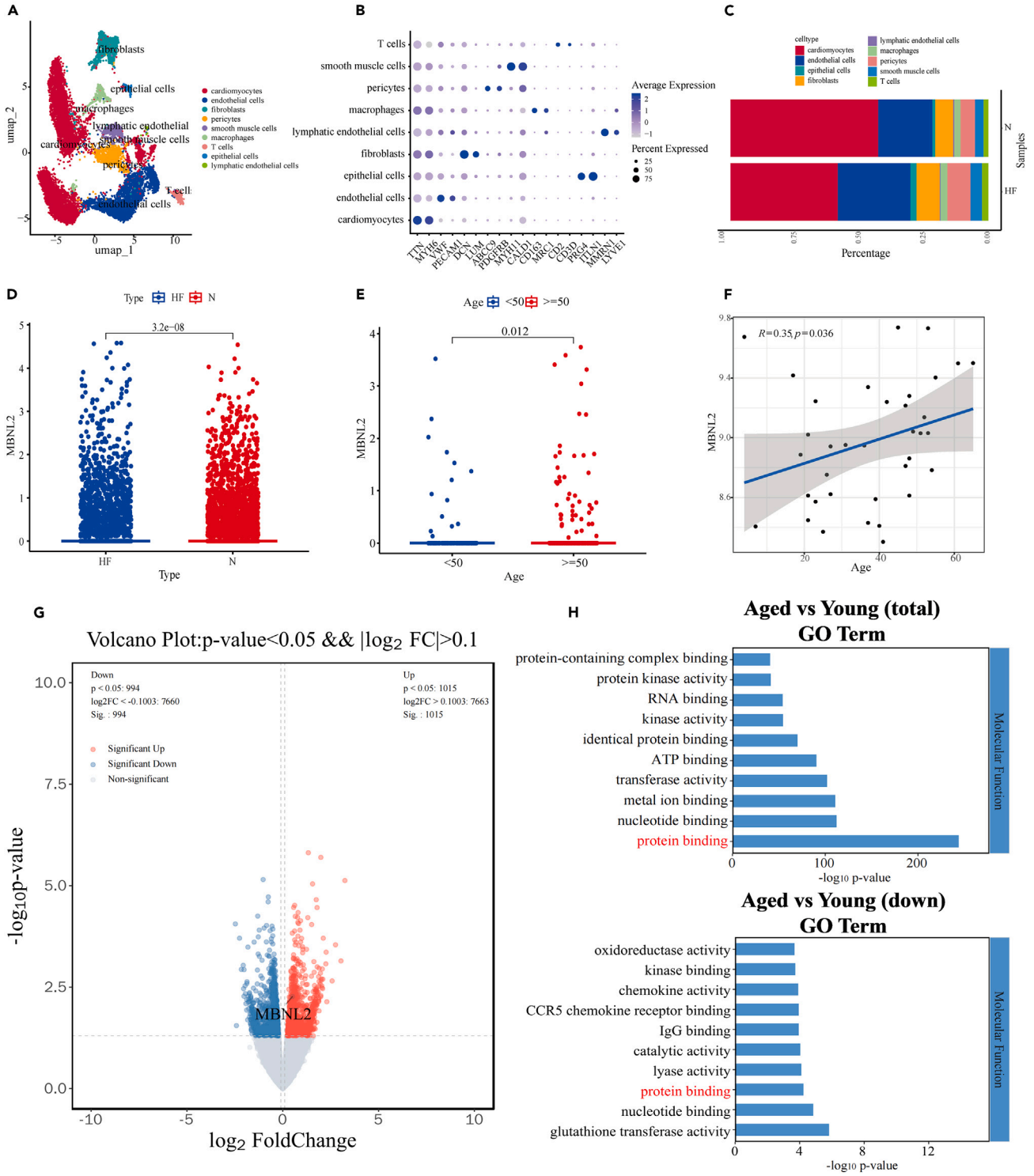

Figure 1. RNA/ScRNA-seq database and RNA/ScRNA-seq analysis about MBNL2

(A) UMAP plots of heart disease profiles of all cells colored by cell types.

(B) Bubble heatmap showing expression levels of chosen signature genes. Dot size implies a fraction of expressing cells, colored based on normalized expression levels.

(C) Horizontal bar chart picturing the relative abundance of various cell types in each type sample.

(D) Scatterplot of all cells in HF and N group.

Figure 1. *Continued*
(E) Scatterplot of fibroblasts about HF samples in <50 and ≥50 group.
(F) Correlation between MBNL2 and age from normal samples in GEO: GSE36961.
(G) Volcano plot of differentially expressed gene.
(H) GO enrichment analysis of DEGs.

SUMOylation of KLF4. Silencing MBNL2 activated the transcription factor KLF4 interact with SUMO1, increasing stability and suppressing the CFs senescence induced by H_2O_2.

Reactive oxygen species, transforming growth factor (TGF)-β activation, and Ang II signaling mediate interstitial and perivascular fibrosis in the senescent heart.[15] TGF-β induces fibroblast activation and differentiation into myofibroblasts that secrete extracellular matrix proteins, which, in turn, cause hypertrophy and fibrosis.[16] In this research, MBNL2 regulates TGF-β1/SMAD3 pathway to playing the important profibrotic function.

In this study, we investigate the role of MBNL2 in aging-related cardiac fibrosis and the mechanism of the MBNL2 profibrotic function. Our results could serve as a valuable guide to clinicians and scientists to help identify target-specific therapeutic agents and construct a better treatment regimen when battling against aging.

RESULTS

Muscleblind-like splicing regulator 2 is upregulated in the old with heart failure

To detect the discrepancy between normal and patients with HF, single-cell RNA-seq data of hearts were obtained from published data with accession number GEO: GSE109816 and GEO: GSE121893. All cells clustered into 9 subsets (Figure 1A) and show the UMAP plots. Then the cell population were annotated with marker genes (Figure 1B). The percentage of cell numbers for different cell types is shown in the normal group and heart failure group (Figure 1C). Then, to detect the correlation between the expression of MBNL2 and aging-related cardiac fibrosis. Firstly, we found that MBNL2 is upregulated in the HF group about all cells (Figure 1D). Then, cardiac fibroblasts about HF samples were studied and found that with the increase of age, the level of MBNL2 elevated significantly in the ≥50 group (Figure 1E). Subsequently, we analyzed the correlated between MBNL2 and age by GEO: GSE36961, we found that MBNL2 is positively correlated with age (Figure 1F). The RNA-seq datasets GEO: GSE207648 analysis result of the volcano plot indicates that MBNL2 was up-regulated in the aged group (Figure 1G). Figure 1H shows the GO analysis significantly annotating to protein binding.

Muscleblind-like splicing regulator 2 expression is upregulated in H_2O_2-treated cardiac fibroblasts and promotes senescence

To examine the effects of MBNL2 in CFs senescence *in vitro*, we used primary cultured neonatal rat cardiac fibroblasts. SA-β-Gal activity assay found H_2O_2 induced the senescence of CFs (Figures 2A and C). As shown in Figures 2B and 2D, the α-SMA-positive area was significantly increased in the H_2O_2-treated group, and H_2O_2 promoted myofibroblast transformation.

To determine the relation between MBNL2 and aging-related cardiac fibrosis, mRNA and protein levels of P21, P16, COLI, COLIII, and MBNL2 were detected by RT-PCR and western blot. The mRNA and protein expression of P21, P16, COLI, COLIII, and MBNL2 significantly increased in the H_2O_2 group (Figures 2E–2G). The increase of MBNL2 levels in H_2O_2-treated cardiac fibroblasts prompted us to figure out whether MBNL2 induces cell senescence and cardiac fibrosis. Then, we overexpressed MBNL2 in CFs, as shown in Figures 2H and 2I, immunofluorescence staining of α-SMA shows that the overexpression of MBNL2 could promote myofibroblasts transformation. Furthermore, the protein expression of P21, P16, COLI, COLIII, and MBNL2 significantly increased in the oe-MBNL2 group (Figures 2J and 2K).

Muscleblind-like splicing regulator 2 expression is increased in cardiac fibroblasts with aging

To validate the increased MBNL2 expression in aged rats, we first established the aged rat models to examine whether cardiac function changed during aging (Figure 3A). Cardiac function deteriorated in aged SD rats and were accompanied by exacerbates the process of cardiac aging, cardiac fibrosis, and microstructural pathologic change in cardiomyocytes. Echocardiography was used to monitor cardiac function (Figure 3B). LVEF (left ventricular ejection fraction), LVFS (left ventricular fractional shortening), LVIDs (left ventricular internal diameter in systole), LVIDd (left ventricular internal diameter in diastolic), LVPWs (left ventricular posterior wall thickness in systole), LVPWd (left ventricular posterior wall thickness in diastole), IVSs (interventricular septal end diastole), and IVSd (interventricular septal end systole) were detected (Figures 3C–3J). Compared to the young group, aged rats decreased LVEF and LVFS, but increased LVIDs. Figure 3K shows an increase in heart size in aging rats. Moreover, we used H&E staining (Figure 3L) to perform histological evaluation, and Masson staining (Figure 3M) of cardiac sections, the results showed disordered cardiac muscle fibers and increased myocardial fibrosis in the aged heart (Figure 3O). HW/BW (mg/g) ratio increased significantly in the aged group (Figure 3N). Then, we detected the upregulation of P21, P16, COLI, and COLIII at both protein and mRNA levels during aged and young rats (Figures 3P–3R). The above results showed that the aging model of rats was successfully constructed.

Furthermore, immunofluorescence staining of Vimentin (red) and MBNL2 (green) was performed in rat hearts, and nuclei were co-stained with DAPI, which shows that MBNL2 was strongly expressed in aged rat cardiac fibroblasts (Figure 3S). The IHC assay shows that MBNL2

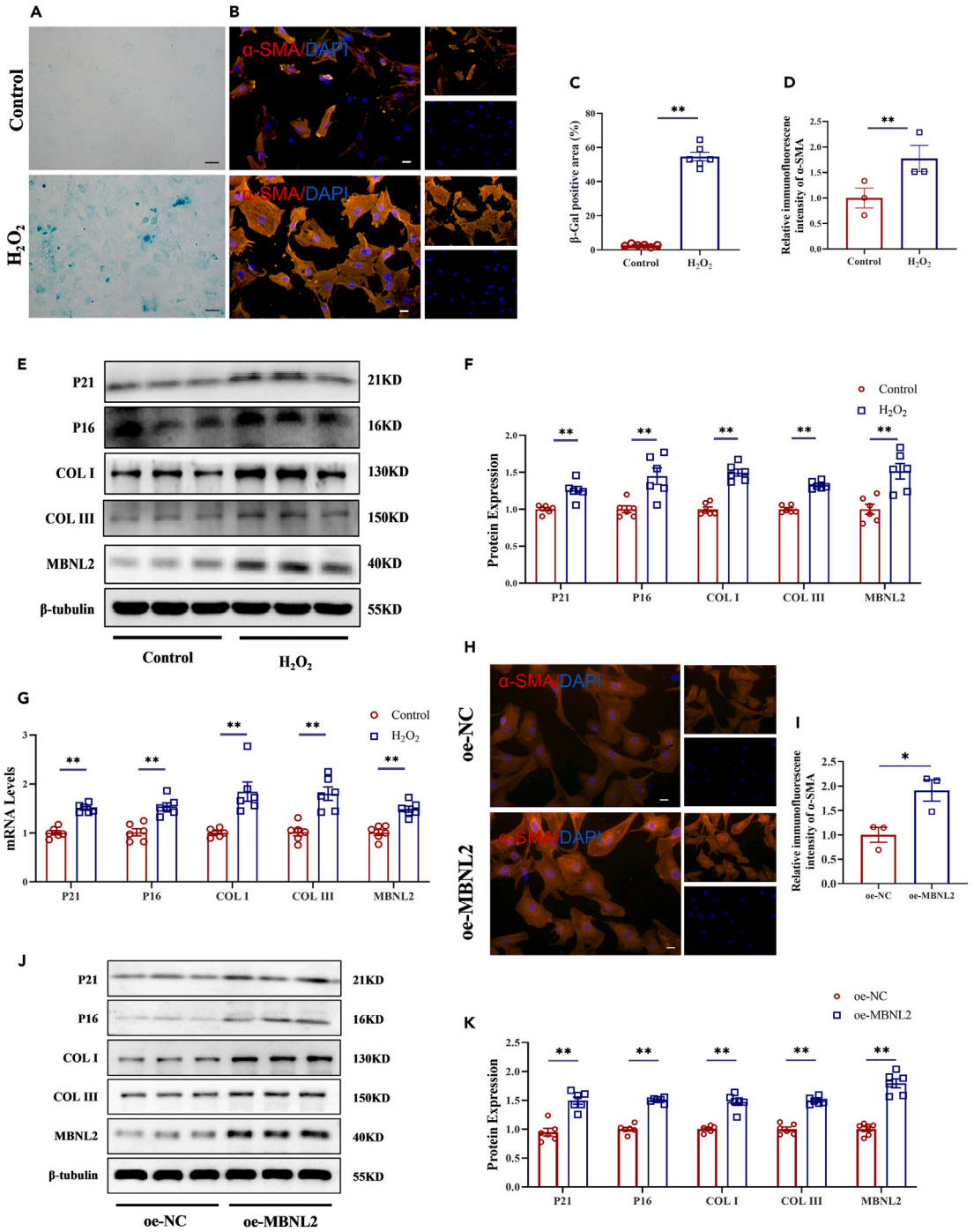

Figure 2. Identification and functional verification of MBNL2 *in vitro*

(A) Representative figure of the SA-β-gal staining. Magnification: 200×; scale bar: 50 μm.

(B) Representative the immunofluorescence of α-SMA. Magnification: 200×; scale bar: 20 μm.

(C) Statistical graph of SA-β-gal staining positive area.

(D) Statistical graph of the immunofluorescence of α-SMA.

(E and F) Representative and statistical graphs of P21, P16, COLI, COLIII, and MBNL2 protein expression.

(G) Relative mRNA level of P21, P16, COLI, COLIII and MBNL2.

(H and I) Representative and statistical graphs of the immunofluorescence of α-SMA. Magnification: 200×; scale bar: 20 μm.

(J and K) Representative and statistical graphs of P21, P16, COLI, COLIII, and MBNL2 protein. (n = 3–6, data are expressed as mean ± SEM, $*p < 0.05$, $**p < 0.01$ vs. the control or oe-NC group).

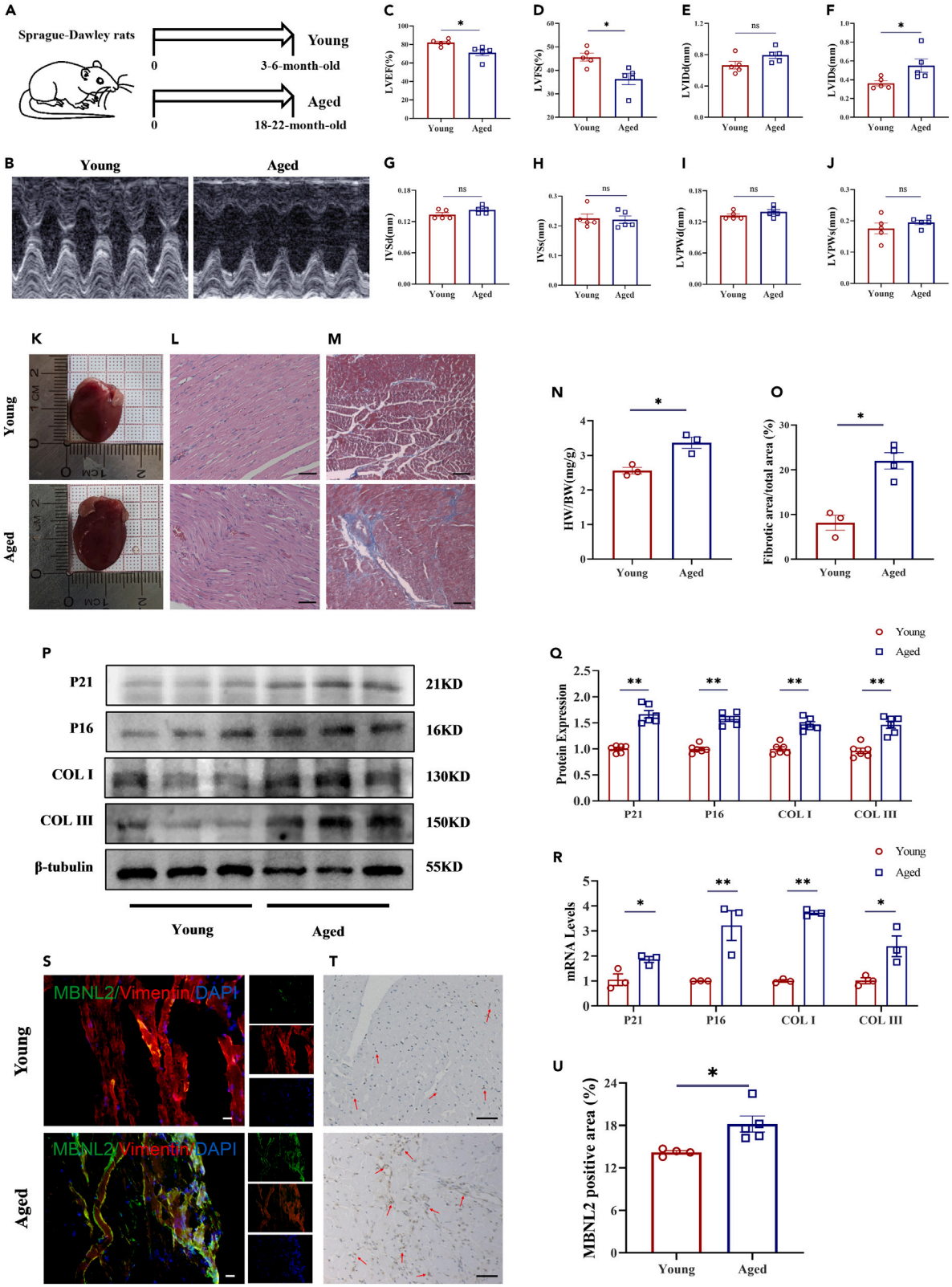
A
Sprague-Dawley rats
Young
0
3-6-month-old
Aged
0
18-22-month-old
B
Young
Aged
C
LVEF(%)
D
LVFS(%)
E
LVIDd(mm)
F
LVIDs(mm)
G
IVSd(mm)
H
IVSs(mm)
I
LVPWd(mm)
J
LVPWs(mm)
K
L
M
N
HW/BW(mg/g)
O
Fibrotic area/total area (%)
P
P21
21KD
P16
16KD
COL I
130KD
COL III
150KD
β-tubulin
55KD
Young
Aged
Q
Protein Expression
R
mRNA Levels
S
MBNL2/Vimentin/DAPI
T
U
MBNL2 positive area (%)

Figure 3. Functional verification of MBNL2 *in vivo*

(A) Schematic of the experimental design.
(B) Representative echocardiographic graphs.
(C–J) Echocardiographic measurements of LVEF, LVFS, LVIDs, LVIDd, LVPWs, LVPWd, IVSs and IVSd.
(K) Gross appearance of the whole heart.
(L) H&E staining of left ventricles. Magnification: 200×; scale bar: 50 μm.
(M) Masson's staining of left ventricles. Magnification: 100×; scale bar: 100 μm.
(N) HW/BW ratio of Young vs. Aged.
(O) Statistical graphs of Masson staining.
(P) Representative graphs of western blot of P21, P16, COLI, and COLIII.
(Q) Quantification of P21, P16, COLI, and COLIII protein levels.
(R) Relative mRNA level of P21, P16, COLI and COLIII.
(S) Representative figure of the immunofluorescence of MBNL2, Vemintin, and DAPI. Magnification: 200×; scale bar: 20 μm
(T and U) Representative images and statistical analysis of IHC staining with MBNL2 antibody. Magnification: 200×; scale bar: 50 μm. (n = 3–6, data are expressed as mean ± SEM, *$p < 0.05$, **$p < 0.01$ vs. the young group).

protein level is expressed at a higher level in the aged rat heart with high fibrosis level than young rat heart (Figures 3T and 3U). These results showed that MBNL2 is up-regulated in cardiac fibroblasts during the cardiac function decreases with aging.

Inhibition of Muscleblind-like splicing regulator 2 decelerates aging-related cardiac fibrosis

Based on the finding that cardiac fibrosis and MBNL2 levels increase with age, we examined the effect of MBNL2 gene silencing on the development of aging-related cardiac fibrosis. Aged rats (18–22 months old) were treated with shMBNL2 or NC once and fed for 4 weeks (Figure 4A). Echocardiography was used to monitor cardiac function (Figure 4B). LVEF, LVFS, LVIDs, LVIDd, LVPWs, LVPWd, IVSs, and IVSd were detected (Figures 4C–4J). HW/BW (mg/g) ratio decreased significantly in Aged +shMBNL2 group vs. Aged +NC group (Figure 4O). H&E and Masson staining of cardiac sections showed that shMBNL2 could decrease disordered cardiac muscle fibers and myocardial fibrosis in an aging heart (Figures 4K, 4L, and 4P). As shown in Figures 4M, 4N, 4Q, and 4R, it found that shMBNL2 in aged rats' hearts could significantly reduce the α-SMA and MBNL2 positive area.

Then, we verified the knockdown efficiency of MBNL2 in the heart (Figure 4S). We detected the expression level of P21, P16, COLI, and COLIII at both protein and mRNA during Young, Aged, Aged + shMBNL2, and Aged + NC groups. The protein and mRNA levels of P21, P16, COLI, and COLIII are increased in Aged group, which is reversed by shMBNL2 (Figures 4T–4V). Therefore, these results suggested that the gene silencing of MBNL2 could reduce aging-related cardiac fibrosis.

Inhibition of Muscleblind-like splicing regulator 2 reduces H_2O_2-induced senescence of cardiac fibroblasts and transformation from fibroblasts to myofibroblasts

Furthermore, to explore the function of MBNL2 in myofibroblast transformation *in vitro*, the collagen gel contraction assays demonstrated that MBNL2 knockdown inhibited the fibroblast contractility (Figures 5A and 5B). Then, immunofluorescence assay investigated α-SMA levels following MBNL2 knockdown after H_2O_2-treated in CFs. As shown in Figures 5C and 5D, sh-MBNL2 significantly decreased the intensity of α-SMA, which increased by H_2O_2. Next, we detected the collagen deposition following MBNL2 knockdown after H_2O_2-treated in CFs. As shown in Figures 5E and 5F, sh-MBNL2 significantly decreased the COL I-positive areas, which increased by H_2O_2.

Then, we detected expression levels of P21, P16, POSTN, COLI, COLIII, and MBNL2 at both protein and mRNA during H_2O_2 and H_2O_2 + sh-MBNL2 group. The protein and mRNA levels of P21, P16, POSTN, COLI, COLIII, and MBNL2 were increased in the H_2O_2 group, which could reversed by sh-MBNL2 (Figures 5G–5I). These results suggested that the silencing of MBNL2 could reduce the senescence of CFs and myofibroblasts' transformation.

Muscleblind-like splicing regulator 2 mediates aging-induced deSUMOylation of Krüppel-like factor 4

Next, we explored the mechanism by which the silencing of MBNL2 reduces myofibroblasts' transformation. It was found that SUMOylation levels were reduced in the aged group and H_2O_2-treated group (Figures 6A and 6B). At the same time, overexpression MBNL2 could downregulate SUMOylation, while knockdown MBNL2 could upreglate SUMOylation (Figures 6C and 6D). Then, we detected the protein level of SENP1 to represent the level of deSUMOylation. As shown in Figures 6E–6G, the protein level of SENP1 was upregulated, and SUMO1 was downregulated after H_2O_2-treated. In the H_2O_2 + sh-MBNL2 group vs. H_2O_2 + NC group, we found that SENP1 was decreased, however, the protein level of KLF4 was without variation (Figures 6H–6J). Recent studies have shown that the SUMOylation of KLF4 plays a crucial role in the regulation of cellular physiological functions. In Figure 6K, CO-IP assay was performed to verify protein interaction between SUMO1 and KLF4, it shows that SUMO1 could be co-precipitated by anti-KLF4 antibody, H_2O_2 decreased this interaction between SUMO1 and KLF4, silencing of MBNL2 increased this interaction.[13,17]

It has been shown that KLF4 mediates the TGF-β1 regulation of cell proliferation and differentiation, and KLF4 inhibits the profibrotic effects of TGF-β1 signaling.[18] Silencing MBNL2 activated the transcription factor KLF4 to interact with SUMO1, increasing stability and suppressing the protein level of TGF-β1 and P-SMAD3 induced by H_2O_2 (Figure 6L–6O).

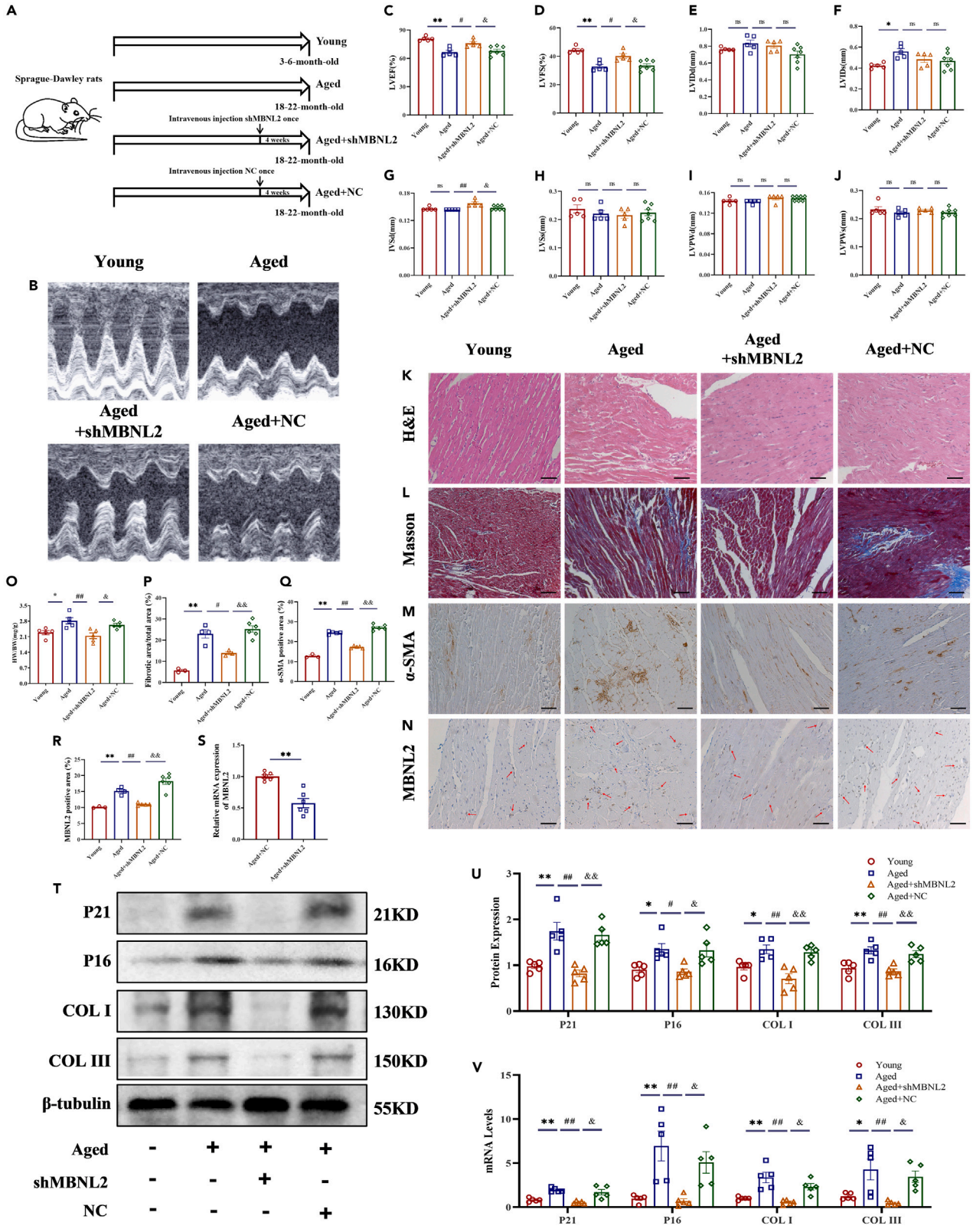
A
Young
3-6-month-old
Sprague-Dawley rats
Aged
18-22-month-old
Intravenous injection shMBNL2 once
4 weeks
Aged+shMBNL2
18-22-month-old
Intravenous injection NC once
4 weeks
Aged+NC
18-22-month-old
B
Young
Aged
Aged +shMBNL2
Aged+NC
C
D
E
F
G
H
I
J
K
H&E
L
Masson
M
α-SMA
N
MBNL2
O
P
Q
R
S
T
P21
P16
COL I
COL III
β-tubulin
21KD
16KD
130KD
150KD
55KD
Aged
shMBNL2
NC
U
Protein Expression
V
mRNA Levels

Figure 4. Inhibition of MBNL2 mitigates aging-related cardiac fibrosis

(A) Schematic of the experimental design.

(B) Representative echocardiographic graphs.

(C–J) Echocardiographic measurements of LVEF, LVFS, LVIDs, LVIDd, LVPWs, LVPWd, IVSs and IVSd.

(K and L) H&E (Magnification: 200×; scale bar: 50 μm) and Masson's (Magnification: 100×; scale bar: 100 μm) staining of left ventricles.

(M and N) Representative images of IHC staining with α-SMA (Magnification: 100×; scale bar: 100 μm) and MBNL2 (Magnification: 200×; scale bar: 50 μm) antibody.

(O) HW/BW ratio.

(P) Percentage of fibrosis area.

(Q and R) Statistical analysis of IHC staining with α-SMA and MBNL2 antibody.

(S). Statistical analysis of MBNL2 mRNA level.

(T and U) Relative western blot representative graphs and quantification of P21, P16, COLI and COLIII protein levels.

(V) Relative mRNA level of P21, P16, COLI and COLIII. (n = 3–7, data are expressed as mean ± SEM, $^{*}p < 0.05$, $^{**}p < 0.01$ vs. the young group, $^{\#}p < 0.05$, $^{\#\#}p < 0.01$ vs. the aged group, $^{\&}p < 0.05$, $^{\&\&}p < 0.01$ vs. the aged+shMBNL2 group).

Muscleblind-like splicing regulator 2 promotes senescence and fibroblast-to-myofibroblast transition on cardiac fibroblasts by regulating TGF-β1/SMAD3 pathway

Next, to validate whether TGF-β1/SMAD3 pathway is regulated by MBNL2, we treated CFs with either over-expression MBNL2 (oe-MBNL2) alone or with the TGF-β1 receptor inhibitor (SB431542) and SMAD3 specific inhibitor (SIS3). We detected the fibrosis function about oe-NC, oe-MBNL2, oe-MBNL2 + SB431542 groups in Figure S1. The immunofluorescence assay (Figures S1A and S1B) investigated α-SMA levels shows that SB431542 significantly decreased the α-SMA intensity, which was increased by oe-MBNL2. And found that SB431542 could reversed the pro-fibrosis effect of oe-MBNL2, downregulated the protein and mRNA expression of POSTN, COLI, and COLIII (Figures S1C–S1E). As shown in Figures 7A, 7B, and S3 significantly decreased the α-SMA intensity, which was increased by oe-MBNL2. The protein levels of P21, P16, POSTN, COLI, COLIII, TGF-β1, MBNL2 and P-SMAD3 were increased in oe-MBNL2 group, which could reversed by SIS3, and the expression of T-SMAD3 was not significantly changed (Figures 7C–7E). The protein and mRNA levels of P21, P16, POSTN, COLI, COLIII TGF-β1, and MBNL2 were also increased in the oe-MBNL2 group, which could reversed by SIS3 (Figures 7F–7G). These results suggest that MBNL2 upregulated the TGF-β1/SMAD3 pathway to promote aged and fibrotic effects on cardiac fibroblasts.

DISCUSSION

Every country in the world is experiencing growth in the proportion of older persons in the population and the treatment of age-related diseases is receiving increasing attention. The incidence of heart failure progressively increases with age, especially heart failure with preserved ejection fraction (HFpEF).[19,20] Therefore, it is important for the elderly to explore the pathogenesis of heart failure and reduce the deterioration of heart failure. In the current study, we identified a substantial role of MBNL2 as an important profibrotic factor in the aged heart. We revealed that MBNL2 could promote aging-related cardiac fibrosis by regulating the deSUMOylation of KLF4 to upregulate the TGF-β1/SMAD3 (Graphical abstract).

The major hallmarks of senescence are mitochondrial dysfunction, genomic instability, telomere attrition, and epigenetic alterations, of which the generation of excess reactive oxygen species (ROS) in mitochondria is responsible for much of the oxidative stress associated with aging.[21] ROS and DNA damage are increased in the H_2O_2-induced cell senescence model, and the expression of the P53/P21 pathway and P16/Rb pathway are upregulated.[22] It was found that H_2O_2-induced senescence in cardiac fibroblasts elevated the expression of cyclin-dependent kinases (CDK) inhibitors such as P16 and P21. MBNL2 belongs to the family of RNA-binding proteins (RBPs), which are alternative splicing factors.[23] At present, multiple age-related diseases have been linked to mutation or altered behavior of RBPs. Knockdown of MBNL2 blocks the cell cycle progression.[24] To explore the role of MBNL2 in cardiofibroblasts senescence, the single-cell RNA-seq data, transcriptomic microarray data, and RNA-seq data analysis results found that MBNL2 level in CFs is related to age and aging could exacerbate the heart failure deterioration. Our research showed that MBNL2 could regulate the expression of CDK inhibitors, such as P21 and P16. Moreover, we found that MBNL2 could affect both mRNA and protein levels of P16 and P21 *in vivo* and *in vitro*, which indicated the participation of MBNL2 in cellular senescence. However, we observed that the protein expression and mRNA level of MBNL2 were no significant differences between young rats' heart and aged rats' heart. Meanwhile, we did not obtained the isolated cardiomyocytes and fibroblasts from the heart of aged rats, and there was no way to directly verify the effect of MBNL2 on CFs *in vivo*.

The fibrosis process is typically ongoing, and cardiac performance deteriorates over time, leading to the eventual death of the patient.[25,26] Fibrosis with the excessive synthesis and deposition of extracellular matrix components in the heart is the main manifestation of aging.[27,28] Aging is also associated with aberrant ECM expression, leading to stiffer, less contractile muscle and aberrant MMPs expression, of which, major components participating in cardiac ECM expansion including COLI and COLIII, play a crucial role that exacerbates the deterioration of heart function the old.[29–32] In this study, we found that the inhibition of MBNL2 could markedly reduce H_2O_2-induced cardiofibroblasts senescence and ECM deposition. *In vivo*, MBNL2 knockdown could exert a cardioprotective effect that diminishes heart size, reduces ECM deposition, and downwards the expression of aging markers. Since cardiac fibrosis is an important pathological factor of heart aging, MBNL2 could be a potential anti-fibrogenic therapeutic target for cardiac aging even in other aging-related diseases.

In pathological states, KLF4 regulates cell fate and differentiation resulting in cardiovascular and inflammation.[33,34] Notably, KLF4 has been reported to be involved in the fibrotic process.[17,35,36] However, there is a dispute between the role of KLF4 in tissue fibrosis about whether

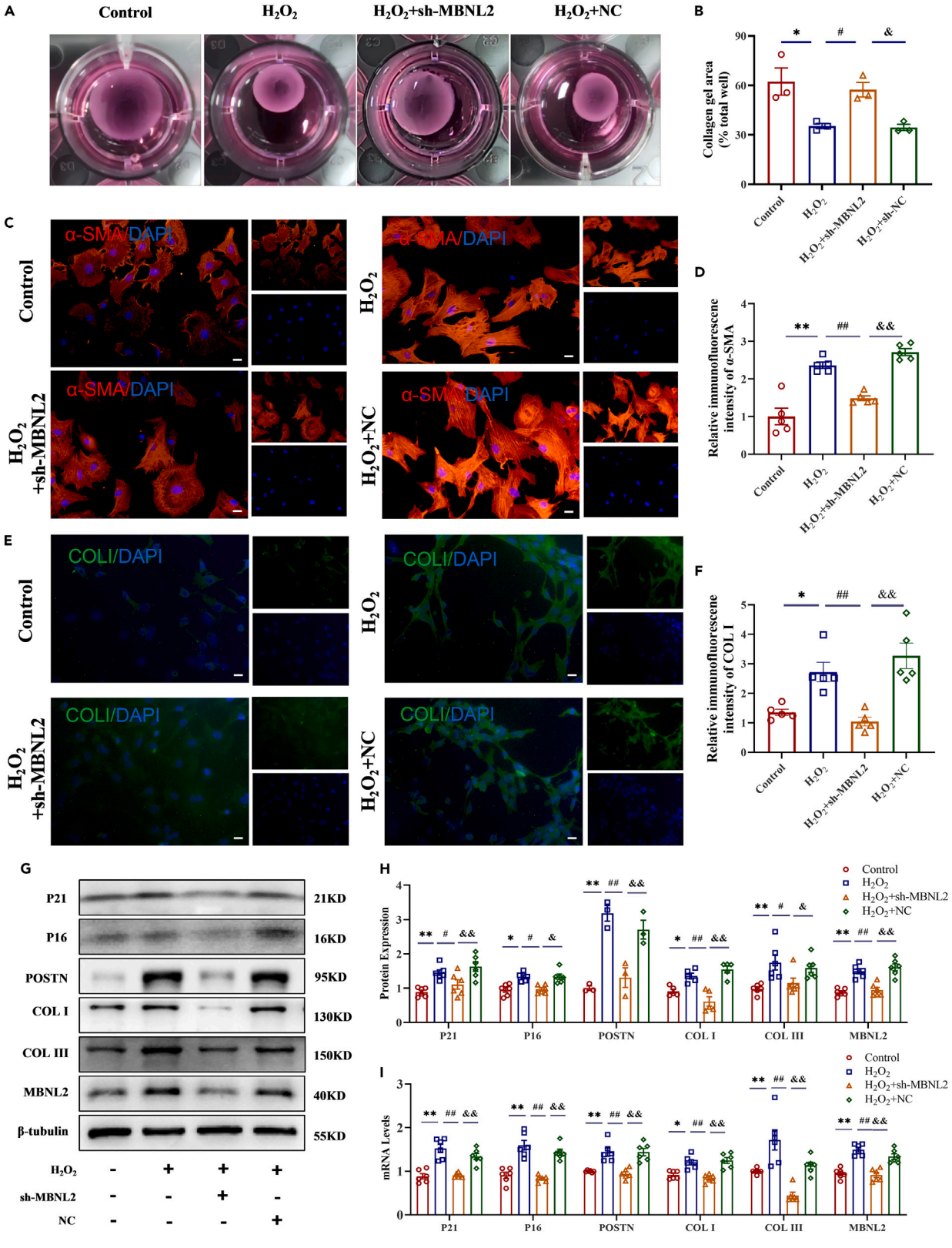
A
Control
H2O2
H2O2+sh-MBNL2
H2O2+NC
B
Collagen gel area (% total well)
C
α-SMA/DAPI
Control
H2O2
H2O2 +sh-MBNL2
H2O2+NC
D
Relative immunofluorescene intensity of α-SMA
E
COLI/DAPI
F
Relative immunofluorescene intensity of COL I
G
P21
P16
POSTN
COL I
COL III
MBNL2
β-tubulin
21KD
16KD
95KD
130KD
150KD
40KD
55KD
sh-MBNL2
NC
H
Protein Expression
I
mRNA Levels

Figure 5. Effects of silencing MBNL2 on cardiac fibroblasts

(A and B) Representative images and statistical graph of collagen gel contraction assay.

(C–F) Representative and statistical graphs of the immunofluorescence of α-SMA and COLI. Magnification: 200×; scale bar: 20 μm.

(G–I) Relative mRNA levels and representative and statistical graphs of P21, P16, POSTN, COLI, COLIII and MBNL2 protein. (n = 3–6, data are expressed as mean ± SEM, *$p < 0.05$, **$p < 0.01$ vs. the control group, $^{\#}p < 0.05$, $^{\#\#}p < 0.01$ vs. the H_2O_2 group, $^{\&}p < 0.05$, $^{\&\&}p < 0.01$ vs. the H_2O_2+sh-MBNL2 group).

KLF4 inhibits or enhances fibroblast differentiation into myofibroblasts by regulating TGF-β. For example, KLF4 expression was reduced in mice with pulmonary fibrosis, and the overexpression of KLF4 inhibited the ability of TGF-β to induce fibroblast differentiation into myofibroblasts.[37] Knockdown of KLF4 inhibits TGF-β expression andinterstitial fibrosis in a model of renal fibrosis.[38] Differences also exist in cardiovascular studies, KLF4 has been reported to the enhanced expression of α-SMA, and promote Ang II-induced cardiac myofibroblast formation through its transcriptional up-regulation of TGF-β1.[39] Conversely, the amelioratation of cardiac dysfunction and fibrosis are associated with restoring KLF4 expression.[40] For another, in our study, the protein level of KLF4 was not significantly changed in the aged model. This result leads us to wonder whether some regulatory mechanisms for KLF4 have not been elucidated or not. Based on previous research, we targeted post-translational modification, especially the SUMOylation.

We used transcriptome sequencing to discuss gene expression in the H_2O_2-induced cardiofibroblasts senescence model. The results showed that MBNL2 was elevated in H_2O_2-induced cardiofibroblasts senescence, and the molecular function of protein binding and identical protein binding were significantly up-regulated. SUMOylation of transcription factors has been shown to affect stability, localization, and activity by altering protein-protein interactions, regulating their subnuclear localization, or inducing conformational changes in the structure of transcription factors.[41] We found that SUMOylation has changed in aged models whether *in vivo* or *in vitro,* but the protein levels of KLF4 were no variation observed in aged models. Some studies suggested that KLF4 can be SUMOylated on individual lysine residues, the main form is the SIM in KLF4 *trans*-activates the target promoters in a SUMO1-dependent manner, and that the lack of SUMO1 is sufficient to repress KLF4 transcriptional activity.[9,12] It has been demonstrated that the activation of α-SMA is mediated by the SUMOylation of KLF4.[42] Similarly, our study found that the silencing of MBNL2 activated SUMOylation of KLF4 and enhanced KLF4 stability, which in turn inhibited the TGF-β1/SMAD3 signaling pathway.

TGF-β/SMAD is a signaling pathway that plays a key role in inflammation, wound healing, and fibrosis, as well as an important trigger for ECM deposition in tissue fibrosis.[43,44] This signaling pathway mainly activates SMAD2/3 through phosphorylation and binds to SMAD4 to form an activated SMAD complex that regulates the transcription of multiple downstream effectors.[45] TGF-β1 can activate the P53/P21 pathway in response to oxidative stress, which results in senescence.[46] SMADs regulate the transcription of TGF-β-responsive genes and activation of P21 or P16.[47] Meanwhile, in this study, both MBNL2 and TGF-β1 play the pro-fibrotic role, so we consider whether the effect of MBNL2 on this age-related cardiac fibrosis occurs by regulating TGF-β-related pathways. Our results found that the inhibition of MBNL2 in the TGF-β1/SMAD3 pathway is associated with cardiofibroblasts senescence and cardiac fibrosis development. CFs were pretreated with SIS3, a specific inhibitor of the SMAD3 pathway, before treating them with oe-MBNL2 found that TGF-β1/SMAD3 pathway-related protein and gene levels were altered and the immunofluorescence expression of α-SMA also changes. And most importantly, after cells treated with SIS3 in the oe-MBNL2 group, we found that P21 and P16 down-regulated compared with the oe-MBNL2 group, this result indicated that MBNL2 may control cell senescence through TGF-β1/SMAD3 pathway of cardiac fibroblasts.

In our study, we revealed the role of MBNL2 as an important profibrotic factor in the aging heart. Our current study identified MBNL2 as a potential therapeutic target in the transformation of cardiac fibroblasts. In conclusion, MBNL2 promoted aging-related cardiac fibrosis by regulating the deSUMOylation of KLF4 to upregulate the TGF-β1/SMAD3 signaling pathway, which may be a promising therapeutic target in related diseases. Finally, a better understanding of cardiac fibroblasts in the aging heart remains critical to addressing and exploring these recurrent questions about myocardial integrity and dysfunction in the elderly heart.

Limitations of the study

Cardiomyocytes and cardiac fibroblasts from aged rats were not isolated to verify the expression of MBNL2 in these two kinds of cells. We demonstrated that MBNL2 plays an important role in promoting cardiac fibrosis and aging by injecting sh-MBNL2 *in vivo* and transfection shRNA *in vitro*. However, this result should be further confirmed by fibroblast-specific MBNL2 knockout mice and MBNL2 knockout cardiac fibroblast cells. The role of MBNL2 in the aging heart should be further studied in the human model. The extent to which KLF4 mediates MBNL2-induced fibrosis should be tested.

STAR★METHODS

Detailed methods are provided in the online version of this paper and include the following:

- KEY RESOURCES TABLE
- RESOURCE AVAILABILITY
  - Lead contact
  - Materials availability
  - Data and code availability
- EXPERIMENTAL MODEL AND STUDY PARTICIPANT DETAILS

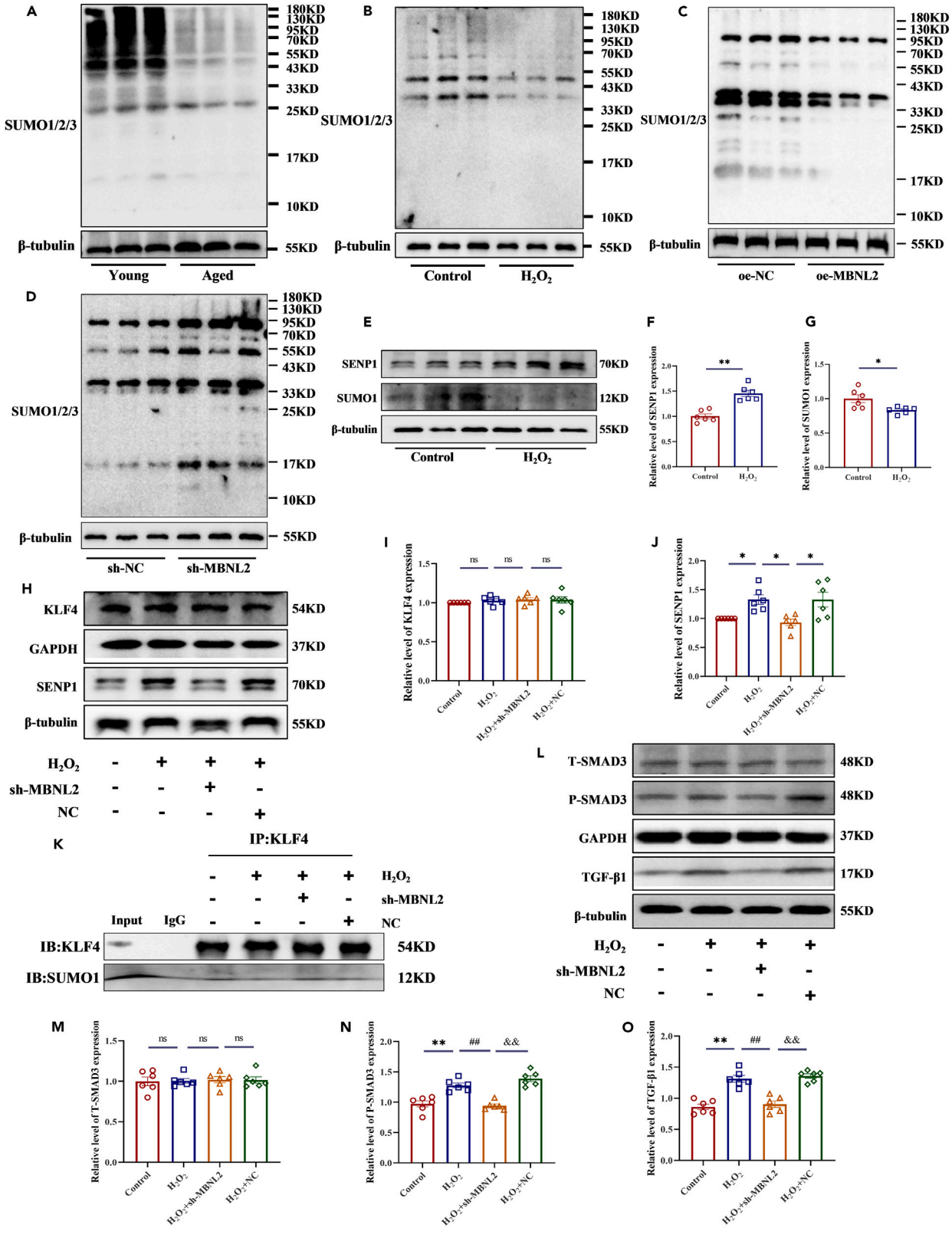
A
SUMO1/2/3
β-tubulin
180KD
130KD
95KD
70KD
55KD
43KD
33KD
25KD
17KD
10KD
55KD
Young
Aged
B
SUMO1/2/3
β-tubulin
Control
H2O2
C
SUMO1/2/3
β-tubulin
oe-NC
oe-MBNL2
D
SUMO1/2/3
β-tubulin
sh-NC
sh-MBNL2
E
SENP1
SUMO1
β-tubulin
70KD
12KD
55KD
F
Relative level of SENP1 expression
G
Relative level of SUMO1 expression
H
KLF4
GAPDH
SENP1
β-tubulin
54KD
37KD
70KD
55KD
H2O2
sh-MBNL2
NC
I
Relative level of KLF4 expression
ns
J
Relative level of SENP1 expression
K
IP:KLF4
Input
IgG
IB:KLF4
IB:SUMO1
54KD
12KD
L
T-SMAD3
P-SMAD3
GAPDH
TGF-β1
β-tubulin
48KD
37KD
17KD
55KD
M
Relative level of T-SMAD3 expression
N
Relative level of P-SMAD3 expression
O
Relative level of TGF-β1 expression
Control
H2O2
H2O2+sh-MBNL2
H2O2+NC

Figure 6. Inhibition of MBNL2 activated SUMOylation of KLF4

(A–D) Representative graphs of SUMO1/2/3 protein in Young vs. Aged, Control vs. H_2O_2, oe-NC vs. oe-MBNL2, sh-NC vs. sh-MBNL2.

(E–G) Representative and statistical graphs of SENP1 and SUMO1 protein.

(H–J) Representative and statistical graphs of KLF4 and SENP1 protein.

(K) Representative immunoblots of KLF4-SUMOylation after incubation with sh-MBNL2 or/and H_2O_2 in CFs (n = 3).

(L–O) Western blot analysis and quantification of TGF-β1, T-SMAD3 and P-SMAD3 protein levels (n = 3–6, data are expressed as mean ± SEM, $^{*}p < 0.05$, $^{**}p < 0.01$ vs. the control group, $^{\#}p < 0.05$, $^{\#\#}p < 0.01$ vs. the H_2O_2 group, $^{\&}p < 0.05$, $^{\&\&}p < 0.01$ vs. the H_2O_2+sh-MBNL2 group).

- Animals experiments
- Cell culture
- METHOD DETAILS
  - *In vivo* MBNL2 knockdown
  - scRNA-seq analysis

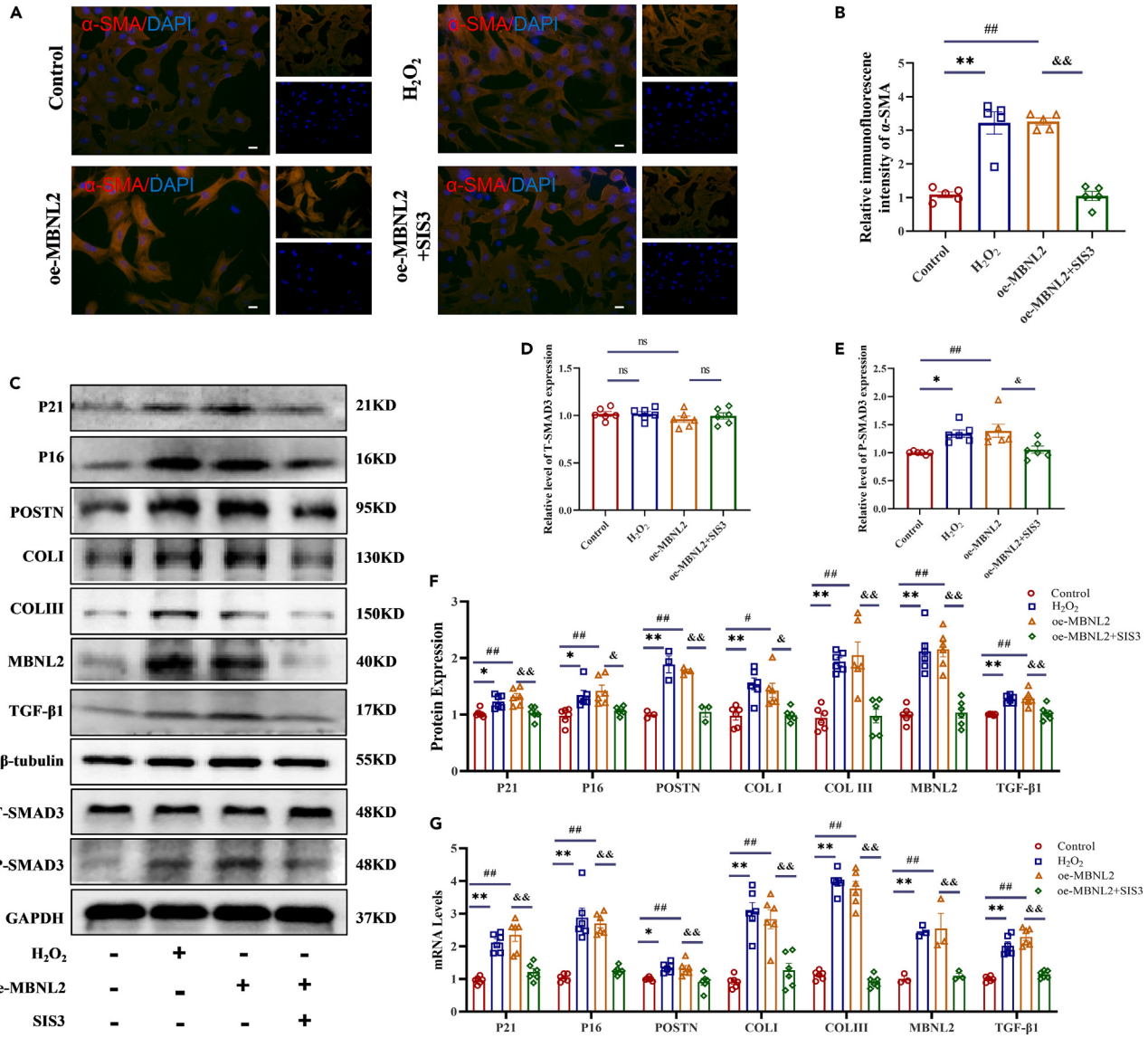

Figure 7. MBNL2 inhibits fibroblast-to-myofibroblast transition through the TGF-β1/SMAD3 pathway *in vitro*

(A and B) Representative and statistical graphs of the immunofluorescence of α-SMA. Magnification: 200×; scale bar: 20 μm.

(C–F) Western blot analysis and quantification of P21, P16, POSTN, COLI, COLIII, MBNL2, TGF-β1, T-SMAD3 and P-SMAD3 protein levels.

(G) Relative mRNA level of P21, P16, POSTN, COLI, COLIII, MBNL2 and TGF-β1 (n = 3–6, data are expressed as mean ± SEM, $^{*}p < 0.05$, $^{**}p < 0.01$ vs. the control group, $^{\#}p < 0.05$, $^{\#\#}p < 0.01$ vs. the control group, $^{\&}p < 0.05$, $^{\&\&}p < 0.01$ vs. the oe-MBNL2 group).

SUPPLEMENTAL INFORMATION

Supplemental information can be found online at https://doi.org/10.1016/j.isci.2024.110163.

ACKNOWLEDGMENTS

The study was funded by the National Natural Science Foundation of China (No. 82170270 and 82370248 to Z.D.); Natural Science Foundation of Heilongjiang Province (YQ2021H015 to Y.G.). Research Project of the First Affiliated Hospital of Harbin Medical University (2021J01 to Z.D., 2021J03 to Y.G. and 2021Y09 to Y.S.).

AUTHOR CONTRIBUTIONS

Conceptualization, J.L., L.W., and Z.D.; methodology, Q.Z. and J.L.; formal analysis, G.L. and Q.C.; investigation, H.W., L.L., M.Y., S.S, and K.Y.; writing – original draft, J.L. and Q.Z.; writing – review and editing, J.L. and Y.S.; visualization, Z.Z. and D.L.; funding acquisition, Y.S., Y.G., and Z.D.; resources, Y.G., and M.L.; supervision, Y.S., Y.G., and Z.D. All authors have read and agreed to the final manuscript.

DECLARATION OF INTERESTS

The authors declare no competing interests.

Received: October 20, 2023
Revised: February 6, 2024
Accepted: May 29, 2024
Published: June 3, 2024

REFERENCES

1. Evangelou, K., Vasileiou, P.V.S., Papaspyropoulos, A., Hazapis, O., Petty, R., Demaria, M., and Gorgoulis, V.G. (2023). Cellular senescence and cardiovascular diseases: moving to the "heart" of the problem. Physiol. Rev. *103*, 609–647. https://doi.org/10.1152/physrev.00007.2022.
2. Triposkiadis, F., Xanthopoulos, A., and Butler, J. (2019). Cardiovascular Aging and Heart Failure: JACC Review Topic of the Week. J. Am. Coll. Cardiol. *74*, 804–813. https://doi.org/10.1016/j.jacc.2019.06.053.
3. Loffredo, F.S., Nikolova, A.P., Pancoast, J.R., and Lee, R.T. (2014). Heart failure with preserved ejection fraction: molecular pathways of the aging myocardium. Circ. Res. *115*, 97–107. https://doi.org/10.1161/CIRCRESAHA.115.302929.
4. Konieczny, P., Stepniak-Konieczna, E., and Sobczak, K. (2014). MBNL proteins and their target RNAs, interaction and splicing regulation. Nucleic Acids Res. *42*, 10873–10887. https://doi.org/10.1093/nar/gku767.
5. Misra, C., Lin, F., and Kalsotra, A. (2018). Deregulation of RNA Metabolism in Microsatellite Expansion Diseases. Adv. Neurobiol. *20*, 213–238. https://doi.org/10.1007/978-3-319-89689-2_8.
6. Czubak, K., Sedehizadeh, S., Kozlowski, P., and Wojciechowska, M. (2019). An Overview of Circular RNAs and Their Implications in Myotonic Dystrophy. Int. J. Mol. Sci. *20*, 4385. https://doi.org/10.3390/ijms20184385.
7. Cai, J., Wang, N., Lin, G., Zhang, H., Xie, W., Zhang, Y., and Xu, N. (2021). MBNL2 Regulates DNA Damage Response via Stabilizing p21. Int. J. Mol. Sci. *22*, 783. https://doi.org/10.3390/ijms22020783.
8. Chothani, S., Schäfer, S., Adami, E., Viswanathan, S., Widjaja, A.A., Langley, S.R., Tan, J., Wang, M., Quaife, N.M., Jian Pua, C., et al. (2019). Widespread Translational Control of Fibrosis in the Human Heart by RNA-Binding Proteins. Circulation *140*, 937–951. https://doi.org/10.1161/CIRCULATIONAHA.119.039596.
9. Ghaleb, A.M., and Yang, V.W. (2017). Krüppel-like factor 4 (KLF4): What we currently know. Gene *611*, 27–37. https://doi.org/10.1016/j.gene.2017.02.025.
10. Sheng, Z., Zhu, J., Deng, Y.-N., Gao, S., and Liang, S. (2021). SUMOylation modification-mediated cell death. Open Biol. *11*, 210050. https://doi.org/10.1098/rsob.210050.
11. Le, N.-T., Martin, J.F., Fujiwara, K., and Abe, J.-I. (2017). Sub-cellular localization specific SUMOylation in the heart. Biochim. Biophys. Acta, Mol. Basis Dis. *1863*, 2041–2055. https://doi.org/10.1016/j.bbadis.2017.01.018.
12. Du, J.X., McConnell, B.B., and Yang, V.W. (2010). A small ubiquitin-related modifier-interacting motif functions as the transcriptional activation domain of Krüppel-like factor 4. J. Biol. Chem. *285*, 28298–28308. https://doi.org/10.1074/jbc.M110.101717.
13. Nie, C.-J., Li, Y.H., Zhang, X.-H., Wang, Z.-P., Jiang, W., Zhang, Y., Yin, W.-N., Zhang, Y., Shi, H.-J., Liu, Y., et al. (2016). SUMOylation of KLF4 acts as a switch in transcriptional programs that control VSMC proliferation. Exp. Cell Res. *342*, 20–31. https://doi.org/10.1016/j.yexcr.2016.03.001.
14. Wang, K., Xiong, J., Lu, Y., Wang, L., and Tian, T. (2023). SENP1-KLF4 signalling regulates LPS-induced macrophage M1 polarization. FEBS J. *290*, 209–224. https://doi.org/10.1111/febs.16589.

15. Biernacka, A., and Frangogiannis, N.G. (2011). Aging and Cardiac Fibrosis. Aging Dis. *2*, 158–173.
16. Dimitrijevic, Z.M., Salinger Martinovic, S.S., Nikolic, V.N., and Cvetkovic, T.P. (2019). Protein Carbonyl Content Is a Predictive Biomarker of Eccentric Left Ventricular Hypertrophy in Hemodialysis Patients. Diagnostics *9*, 202. https://doi.org/10.3390/diagnostics9040202.
17. Ke, B., Zhang, A., Wu, X., and Fang, X. (2015). The Role of Krüppel-like Factor 4 in Renal Fibrosis. Front. Physiol. *6*, 327. https://doi.org/10.3389/fphys.2015.00327.
18. Mreich, E., Chen, X.-M., Zaky, A., Pollock, C.A., and Saad, S. (2015). The role of Krüppel-like factor 4 in transforming growth factor-β-induced inflammatory and fibrotic responses in human proximal tubule cells. Clin. Exp. Pharmacol. Physiol. *42*, 680–686. https://doi.org/10.1111/1440-1681.12405.
19. Vilaro, J.R. (2023). Heart Failure with Preserved Ejection Fraction: Important Things to Know About the Stiff Heart. Cardiovasc. Innov. Appl. *8*, 954. https://doi.org/10.15212/CVIA.2023.0058.
20. Ijaz, N., Buta, B., Xue, Q.-L., Mohess, D.T., Bushan, A., Tran, H., Batchelor, W., deFilippi, C.R., Walston, J.D., Bandeen-Roche, K., et al. (2022). Interventions for Frailty Among Older Adults With Cardiovascular Disease: JACC State-of-the-Art Review. J. Am. Coll. Cardiol. *79*, 482–503. https://doi.org/10.1016/j.jacc.2021.11.029.
21. López-Otín, C., Blasco, M.A., Partridge, L., Serrano, M., and Kroemer, G. (2023). Hallmarks of aging: An expanding universe. Cell *186*, 243–278. https://doi.org/10.1016/j.cell.2022.11.001.
22. Wang, Z., Wei, D., and Xiao, H. (2013). Methods of cellular senescence induction using oxidative stress. Methods Mol. Biol. *1048*, 135–144. https://doi.org/10.1007/978-1-62703-556-9_11.
23. Zhang, B.-W., Cai, H.-F., Wei, X.-F., Sun, J.-J., Lan, X.-Y., Lei, C.-Z., Lin, F.-P., Qi, X.-L., Plath, M., and Chen, H. (2016). miR-30-5p Regulates Muscle Differentiation and Alternative Splicing of Muscle-Related Genes by Targeting MBNL. Int. J. Mol. Sci. *17*, 182. https://doi.org/10.3390/ijms17020182.
24. Perron, G., Jandaghi, P., Solanki, S., Safisamghabadi, M., Storoz, C., Karimzadeh, M., Papadakis, A.I., Arseneault, M., Scelo, G., Banks, R.E., et al. (2018). A General Framework for Interrogation of mRNA Stability Programs Identifies RNA-Binding Proteins that Govern Cancer Transcriptomes. Cell Rep. *23*, 1639–1650. https://doi.org/10.1016/j.celrep.2018.04.031.
25. Ongstad, E.L., and Gourdie, R.G. (2016). Can heart function lost to disease be regenerated by therapeutic targeting of cardiac scar tissue? Semin. Cell Dev. Biol. *58*, 41–54. https://doi.org/10.1016/j.semcdb.2016.05.020.
26. Dimza, M., and Aranda, J.M. (2023). Heart Failure Guideline Directed Medical Therapy: Which One and When? Cardiovasc. Innov. Appl. *8*, 936. https://doi.org/10.15212/CVIA.2023.0077.
27. Huang, P., Bai, L., Liu, L., Fu, J., Wu, K., Liu, H., Liu, Y., Qi, B., and Qi, B. (2021). Redd1 knockdown prevents doxorubicin-induced cardiac senescence. Aging (Albany NY) *13*, 13788–13806. https://doi.org/10.18632/aging.202972.
28. Zhang, Y., and Wang, J. (2023). Cellular and Molecular Mechanisms in Idiopathic Pulmonary Fibrosis. Adv. Respir. Med. *91*, 26–48. https://doi.org/10.3390/arm91010005.
29. Dasgupta, J., Kar, S., Liu, R., Joseph, J., Kalyanaraman, B., Remington, S.J., Chen, C., and Melendez, J.A. (2010). Reactive oxygen species control senescence-associated matrix metalloproteinase-1 through c-Jun-N-terminal kinase. J. Cell. Physiol. *225*, 52–62. https://doi.org/10.1002/jcp.22193.
30. Sessions, A.O., Kaushik, G., Parker, S., Raedschelders, K., Bodmer, R., Van Eyk, J.E., and Engler, A.J. (2017). Extracellular matrix downregulation in the Drosophila heart preserves contractile function and improves lifespan. Matrix Biol. *62*, 15–27. https://doi.org/10.1016/j.matbio.2016.10.008.
31. Rodríguez, C., and Martínez-González, J. (2019). The Role of Lysyl Oxidase Enzymes in Cardiac Function and Remodeling. Cells *8*, 1483. https://doi.org/10.3390/cells8121483.
32. Ezeani, M., Noor, A., Alt, K., Lal, S., Donnelly, P.S., Hagemeyer, C.E., and Niego, B. (2021). Collagen-Targeted Peptides for Molecular Imaging of Diffuse Cardiac Fibrosis. J. Am. Heart Assoc. *10*, e022139. https://doi.org/10.1161/JAHA.121.022139.
33. Yamanaka, S. (2008). Induction of pluripotent stem cells from mouse fibroblasts by four transcription factors. Cell Prolif. *41*, 51–56. https://doi.org/10.1111/j.1365-2184.2008.00493.x.
34. Yang, S., Cui, H., Xie, N., Icyuz, M., Banerjee, S., Antony, V.B., Abraham, E., Thannickal, V.J., and Liu, G. (2013). miR-145 regulates myofibroblast differentiation and lung fibrosis. FASEB J *27*, 2382–2391. https://doi.org/10.1096/fj.12-219493.
35. Ghaleb, A.M., Nandan, M.O., Chanchevalap, S., Dalton, W.B., Hisamuddin, I.M., and Yang, V.W. (2005). Krüppel-like factors 4 and 5: the yin and yang regulators of cellular proliferation. Cell Res. *15*, 92–96. https://doi.org/10.1038/sj.cr.7290271.
36. Wang, J., Zhao, M., Zhang, H., Yang, F., Luo, L., Shen, K., Wang, X., Li, Y., Zhang, J., Zhang, J., et al. (2022). KLF4 Alleviates Hypertrophic Scar Fibrosis by Directly Activating BMP4 Transcription. Int. J. Biol. Sci. *18*, 3324–3336. https://doi.org/10.7150/ijbs.71167.
37. Penke, L.R., Speth, J.M., Huang, S.K., Fortier, S.M., Baas, J., and Peters-Golden, M. (2022). KLF4 is a therapeutically tractable brake on fibroblast activation that promotes resolution of pulmonary fibrosis. JCI Insight *7*, e160688. https://doi.org/10.1172/jci.insight.160688.
38. Xu, D., Chen, P.-P., Zheng, P.-Q., Yin, F., Cheng, Q., Zhou, Z.-L., Xie, H.-Y., Li, J.-Y., Ni, J.-Y., Wang, Y.-Z., et al. (2021). KLF4 initiates sustained YAP activation to promote renal fibrosis in mice after ischemia-reperfusion kidney injury. Acta Pharmacol. Sin. *42*, 436–450. https://doi.org/10.1038/s41401-020-0463-x.
39. Zhang, Y., Wang, Y., Liu, Y., Wang, N., Qi, Y., and Du, J. (2013). Krüppel-like factor 4 transcriptionally regulates TGF-β1 and contributes to cardiac myofibroblast differentiation. PLoS One *8*, e63424. https://doi.org/10.1371/journal.pone.0063424.
40. Lee, C., Cho, S., and Jeong, D. (2023). Inhibition of miR-25 Ameliorates Cardiac Dysfunction and Fibrosis by Restoring Krüppel-like Factor 4 Expression. Int. J. Mol. Sci. *24*, 12434. https://doi.org/10.3390/ijms241512434.
41. Yu, X., Lao, Y., Teng, X.-L., Li, S., Zhou, Y., Wang, F., Guo, X., Deng, S., Chang, Y., Wu, X., et al. (2018). SENP3 maintains the stability and function of regulatory T cells via BACH2 deSUMOylation. Nat. Commun. *9*, 3157. https://doi.org/10.1038/s41467-018-05676-6.
42. Kawai-Kowase, K., Ohshima, T., Matsui, H., Tanaka, T., Shimizu, T., Iso, T., Arai, M., Owens, G.K., and Kurabayashi, M. (2009). PIAS1 mediates TGFbeta-induced SM alpha-actin gene expression through inhibition of KLF4 function-expression by protein sumoylation. Arterioscler. Thromb. Vasc. Biol. *29*, 99–106. https://doi.org/10.1161/ATVBAHA.108.172700.
43. Weng, L., Jia, S., Xu, C., Ye, J., Cao, Y., Liu, Y., and Zheng, M. (2018). Nogo-C regulates post myocardial infarction fibrosis through the interaction with ER Ca2+ leakage channel Sec61α in mouse hearts. Cell Death Dis. *9*, 612. https://doi.org/10.1038/s41419-018-0598-6.
44. Deluque, A.L., Oliveira, B.M., Souza, C.S., Maciel, A.L.D., Francescato, H.D.C., Giovanini, C., de Almeida, L.F., de Paula, F.J.A., Costa, R.S., Antunes-Rodrigues, J., and Coimbra, T.M. (2022). Paricalcitol Improves the Angiopoietin/Tie-2 and VEGF/VEGFR2 Signaling Pathways in Adriamycin-Induced Nephropathy. Nutrients *14*, 5316. https://doi.org/10.3390/nu14245316.
45. Sulaiman, A., Chambers, J., Chilumula, S.C., Vinod, V., Kandunuri, R., McGarry, S., and Kim, S. (2022). At the Intersection of Cardiology and Oncology: TGFβ as a Clinically Translatable Therapy for TNBC Treatment and as a Major Regulator of Post-Chemotherapy Cardiomyopathy. Cancers *14*, 1577. https://doi.org/10.3390/cancers14061577.
46. Samarakoon, R., Higgins, S.P., Higgins, C.E., and Higgins, P.J. (2019). The TGF-β1/p53/PAI-1 Signaling Axis in Vascular Senescence: Role of Caveolin-1. Biomolecules *9*, 341. https://doi.org/10.3390/biom9080341.
47. Vijayachandra, K., Higgins, W., Lee, J., and Glick, A. (2009). Induction of p16ink4a and p19ARF by TGFbeta1 contributes to growth arrest and senescence response in mouse keratinocytes. Mol. Carcinog. *48*, 181–186. https://doi.org/10.1002/mc.20472.
48. Wang, L., Yu, P., Zhou, B., Song, J., Li, Z., Zhang, M., Guo, G., Wang, Y., Chen, X., Han, L., and Hu, S. (2020). Single-cell reconstruction of the adult human heart during heart failure and recovery reveals the cellular landscape underlying cardiac function. Nat. Cell Biol. *22*, 108–119. https://doi.org/10.1038/s41556-019-0446-7.
49. Bos, J.M., Hebl, V.B., Oberg, A.L., Sun, Z., Herman, D.S., Teekakirikul, P., Seidman, J.G., Seidman, C.E., Dos Remedios, C.G., Maleszewski, J.J., et al. (2020). Marked Up-Regulation of ACE2 in Hearts of Patients With Obstructive Hypertrophic Cardiomyopathy: Implications for SARS-CoV-2-Mediated COVID-19. Mayo Clin. Proc. *95*, 1354–1368. https://doi.org/10.1016/j.mayocp.2020.04.028.
50. Berkowicz, P., Totoń-Żurańska, J., Kwiatkowski, G., Jasztal, A., Csípő, T., Kus, K., Tyrankiewicz, U., Orzyłowska, A., Wołkow, P., Tóth, A., and Chlopicki, S. (2023). Accelerated ageing and coronary microvascular dysfunction in chronic heart failure in

Tgαq*44 mice. Geroscience *45*, 1619–1648. https://doi.org/10.1007/s11357-022-00716-y.

51. Feng, Y., Xu, W., Zhang, W., Wang, W., Liu, T., and Zhou, X. (2019). LncRNA DCRF regulates cardiomyocyte autophagy by targeting miR-551b-5p in diabetic cardiomyopathy. Theranostics *9*, 4558–4566. https://doi.org/10.7150/thno.31052.

52. Su, M., Wang, J., Wang, C., Wang, X., Dong, W., Qiu, W., Wang, Y., Zhao, X., Zou, Y., Song, L., et al. (2015). MicroRNA-221 inhibits autophagy and promotes heart failure by modulating the p27/CDK2/mTOR axis. Cell Death Differ. *22*, 986–999. https://doi.org/10.1038/cdd.2014.187.

53. Shan, H., Li, T., Zhang, L., Yang, R., Li, Y., Zhang, M., Dong, Y., Zhou, Y., Xu, C., Yang, B., et al. (2019). Heme oxygenase-1 prevents heart against myocardial infarction by attenuating ischemic injury-induced cardiomyocytes senescence. EBioMedicine *39*, 59–68. https://doi.org/10.1016/j.ebiom.2018.11.056.

STAR★METHODS

KEY RESOURCES TABLE

REAGENT or RESOURCE	SOURCE	IDENTIFIER
Antibodies		
Anti-GAPDH antibody	Proteintech	Cat# 60004-1-Ig; RRID:AB_2107436
Anti-β-Tubulin antibody	Proteintech	Cat# 66240-1-Ig; RRID:AB_2881629
Anti-P21 antibody	Proteintech	Cat# 10355-1-AP; RRID:AB_2077682
Anti-P16 antibody	SANTA	Cat# sc-1661; RRID:AB_628067
Anti-COL I antibody	Proteintech	Cat# 66761-1-Ig; RRID:AB_2882107
Anti-COL III antibody	Proteintech	Cat# 22734-1-AP; RRID:AB_2879158
Anti-MBNL2 antibody	SANTA	Cat# sc-136167; RRID:AB_2140469
Anti-α-SMA antibody	Abcam	Cat# ab124964; RRID:AB_11129103
Anti-T-SMAD3 antibody	Affinity Biosciences	Cat# AF6362; RRID:AB_2835210
Anti-P-SMAD3 antibody	Affinity Biosciences	Cat# AF3362; RRID:AB_2834777
Anti-TGF-β1 antibody	Abcam	Cat# ab215715; RRID:AB_2893156
Anti-SENP1 antibody	Proteintech	Cat# 25349-1-AP; RRID:AB_2880039
Anti-KLF4 antibody	Proteintech	Cat# 11880-1-AP; RRID:AB_10640807
Anti-SUMO1 antibody	Proteintech	Cat# 10329-1-AP; RRID:AB_2286872
Anti-SUMO1/2/3 antibody	PTM BIO	Cat# PTM-1109
Anti-POSTN antibody	ABclonal Technology Co., Ltd.	Cat# A14556; RRID : AB_2761432
Anti-Vimentin antibody	Proteintech	Cat# 10366-1-AP; RRID : AB_2273020
Biological samples		
SD Rats	Beijing VitalRiver Laboratory Animal Technology Co, Ltd	NA
Chemicals, peptides, and recombinant proteins		
H_2O_2	Millipore	Cat# 88597
SIS3	MedChemExpress	Cat# HY-13013
SB431542	MedChemExpress	Cat# HY-10431
Critical commercial assays		
jetPRIME	Polyplus	Cat# 101000046
TRIzol reagent	Haigene	Cat# B0201
H&E staining kit	Solarbio	Cat# G1120
Masson's trichrome stain kit	Solarbio	Cat# G1340
Senescence β-Galactosidase Staining Kit	CST	Cat# 9860S
Hifair® III 1st Strand cDNA Synthesis SuperMix for qPCR	Yeasen	Cat# 11141ES60
Hieff UNICON® Universal Blue qPCR SYBR Green Master Mix	Yeasen	Cat# 11184ES08
Cell Contraction Assays, Two-Step Attached Model	Cell Biolabs	Cat# CBA-201
Protein A/G Magnetic Beads	MedChemExpress	Cat# HY-K0202
Plasmid Extraction Kit	Seven	Cat# SM282-01
Deposited data		
RNA sequences data	https://www.ncbi.nlm.nih.gov/geo/	GSE207648

(*Continued on next page*)

Continued

REAGENT or RESOURCE	SOURCE	IDENTIFIER
scRNA-seq data	https://www.ncbi.nlm.nih.gov/geo/	GSE109816 or GSE121893
transcriptomic microarray data	https://www.ncbi.nlm.nih.gov/geo/	GSE36961
Oligonucleotides		
GAPDH-F	this manuscript	5′-ACTCCCATTCTTCCACCTTTG-3′;
GAPDH-R	this manuscript	5′-CCCTGTTGCTGTAGCCATATT-3′;
P16-F	this manuscript	5′-CCGATACAGGTGAT GATGATGG-3′;
P16-R	this manuscript	5′-CAGTACTACCAGAGTGTCTAGGA-3′;
P21-F	this manuscript	5′-GCACTCTGAAGATGTGCCTATG-3′;
P21-R	this manuscript	5′-CCCATAACTCCTTGCTAAC TCC-3′;
MBNL2-F	this manuscript	5′-ACCACACCTGTCATTGTTCC-3′;
MBNL2-R	this manuscript	5′-CCCTGC ATACCTCCAGTTTATC-3′;
COL I-F	this manuscript	5′-CTGACGCATGGCCAAGAAGA-3′;
COL I-R	this manuscript	5′-GTGCCATTGTGGCAGATACAG-3′;
COL III-F	this manuscript	5′-CTGAACTCAAGAGCG GAGAATAC-3′;
COL III-R	this manuscript	5′-CAGTCATGGGACTGGCATTTA-3′;
TGF-β1-F	this manuscript	5′-CTGAACCAAGGAGACGGAATAC-3′;
TGF-β1-R	this manuscript	5′- GTTTGGGACTGATCCC ATTGA-3′;
POSTN-F	this manuscript	5′-TAAGTTCGTTCGTGGCAGCA-3′;
POSTN-R	this manuscript	5′-AGGCTGAAGACTGCCTTGAAT-3′.
Software and algorithms		
GraphPad Prism 9.0	GraphPad	https://www.graphpad.com/
ImageJ	NIH	https://imagej.nih.gov/ij/

RESOURCE AVAILABILITY

Lead contact

Further information and requests for resources and reagents should be directed to and will be fulfilled by the lead contact, Zengxiang Dong (dongzx@hrbmu.edu.cn).

Materials availability

This study did not generate new unique reagents.

Data and code availability

The RNA sequences data, scRNA-seq data and transcriptomic microarray data that reported in this paper have been deposited at GEO, which are publicly available as of the date of publication. Accession numbers are listed in the key resources table.

This paper does not report original code.

Any additional information required to reanalyze the data reported in this paper is available from the lead contact upon request.

EXPERIMENTAL MODEL AND STUDY PARTICIPANT DETAILS

Animals experiments

The animal experiments in this study were conducted by the Guide for the Care and Use of Laboratory Animals and approved by the Institutional Animal Care and Use Committee of the First Affiliated Hospital of Harbin Medical University (IACUC No. 2021109). Male SD rats were purchased from Beijing VitalRiver Laboratory Animal Technology Co, Ltd (Beijing, China) and raised at the Experimental Animal Center of the First Affiliated Hospital of Harbin Medical University. The rats were individually housed under 12:12-h light-dark cycles and were offered water and food *ad libitum*. Defined 3–6 months old rats were young group and 18–22 months old as aged group. At the end of the feeding regimen, the rats were anesthetized with 3% pentobarbital sodium and sacrificed by deep anesthesia of pentobarbital sodium.

Cell culture

Primary rat cardiomyocytes were cultured as previously described.[52] Cardiac fibroblasts (CFs) were acutely isolated from neonatal SD rats (1-3-day-old). CFs cells were cultured under standard conditions (37°C, 5% CO_2). The cells were divided into different groups and subjected to experimental procedures at 80% confluence. According to the experimental group, CFs were treated with 50 μM H_2O_2 for 48 h at 37°C to make CFs senescence.[53]

METHOD DETAILS

In vivo MBNL2 knockdown

In a separate set of experiments, rats were randomly assigned to three experimental groups to investigate the effect of MBNL2 knockdown in aging-related cardiac fibrosis. Knockdown of the MBNL2 virus was constructed by Shanghai Genechem Co. using the recombinant serum type 9 adeno-associated virus system (AAV9) and the empty vector as the negative control. The shRNA was generated after cloning target sequence of MBNL2 (GCGTTGCATGAGGGAGAAATG) into the adeno-associated virus vector GV478 (Shanghai Genechem Co., Ltd). The virus was injected into 18–20 months old SD rats via the tail vein for four weeks.

scRNA-seq analysis

We obtained a scRNA-seq dataset of normal heart and heart disease (GSE109816 and GSE121893) from Gene Expression Omnibus (GEO) (https://www.ncbi.nlm.nih.gov/geo/).[48] The R package "Seurat" is used to create objects. Filter out low-quality cells based on mitochondrial RNA percentage and number of genes per cell. Then, we used the "harmony" algorithm to merge the 20 samples (14 normal and 6 heart failure), the data were normalized to obtain the top 3,000 highly variable genes, performed principal component analysis (PCA) filtering on the data. FindMarkers ('logfc.threshold' = 0.25 and 'min.pct' = 0.25, Wilcoxon rank-sum test) was used to find differentially expressed genes among these cell clusters, using marker genes to annotate cell clusters as known cell types.

Spearman correlation analysis

The transcriptomic microarray dataset (GSE36961) of 36 normal human heart tissues with complete clinical information was obtained from the GEO database.[49] Gene expression levels and clinical information were extracted after standardizing the data, and correlation analysis was performed using spearman.

Transcriptome datasets and bioinformatics analysis

We obtained an RNA-seq dataset of Young and Aged mice heart (GSE207648) from GEO.[50] Young (GSM6304319, GSM6304320, GSM6304321, GSM6304322, and GSM6304323) and Aged (GSM6304329, GSM6304330, GSM6304331, GSM6304332, GSM6304333) were used the R package ''limma'' to calculate statistical changes in expression levels. The genes with standards of p-value < 0.05 and $|log2FC| \geq 0.1$ were considered as DEGs. The volcano map and GO analysis were drawn based on the R (https://www.r-project.org/) on the OECloud platform (https://cloud.oebiotech.com/task/).

Echocardiographic measurement

Echocardiography of cardiac structure and function was determined as previously reported.[51] Rats were anesthetized and the evaluation of cardiac function was achieved by the Vevo770 animal ultrasound imaging system (Visual Sonics, Canada).

Histological analysis

Histological analysis of rats' hearts was determined with H&E or Masson method. The heart tissues were fixed in 4% paraformaldehyde for 2 days, embedded in paraffin, and sliced into 4 μm sections. H&E staining kit (Solarbio, G1120, China) and Masson's trichrome stain kit (Solarbio, G1340, China) were used to measure cardiomyocyte morphology and cardiac fibrosis. The myocardial sections were observed by microscope (Carl Zeiss Co. Ltd., USA).

Immunohistochemistry assays (IHC)

Rats' heart tissue sections were deparaffinized in xylene series and rehydrated through ethanol series, followed by the treatment of sections with 3% H_2O_2 for 10 min. The sections were heated with antigen retrieval buffers to repair the antigen. Then they were blocked with 5% bovine serum albumin at 37°C for 1 h. Sections were subjected to antigen retrieval in citrate buffer before adding MBNL2 primary antibody (Santa Cruz, sc-136167, USA), COLI primary antibody (Abcam, ab37410, Great Britain), and α-SMA (Abcam, ab124964, Great Britain) overnight at 4°C. The following day, the sections were incubated with horseradish peroxidase (HRP)-conjugated anti-mouse antibody or anti-rabbit antibody and stained with diaminobenzidine (DAB). Images were taken with the microscope (Carl Zeiss Co. Ltd., USA).

Senescence related β-galactosidase (SA-β-gal) activity assay

β-galactosidase activity was tested by a commercial kit (CST, 9860S, USA). First, the cultured cells or tissue sections were fixed with the fixation solution. Then, the fixed cells or tissue sections were washed three times with PBS. The cultured cells were next incubated with the staining

solution at 37°C. The images of stained cells were taken by the inverted microscope (Carl Zeiss Co. Ltd., USA). The fixative solution and staining solution were provided in the kit.

Construction of plasmids and transfection

The overexpression plasmid of MBNL2 (NM_001111064) was constructed with the CV702 vector (CMV enhancer-MCS-3FLAG-SV40-Puromycin). And GV101 vector (hU6-MCS-SV40-Neomycin) containing GGTCCCACCATAGGGACAAAT sequence to knockdown MBNL2, further the empty vector was purchased from GeneChem (Shanghai Genechem Co., Ltd). The plasmid DNA was purified using the SM282-01 plasmid extraction kit (Seven, Beijing, China) to obtain the plasmids. After CFs had grown to 80% confluence on a 60 mm dish, transfection was accomplished by using jetPRIME (Polyplus, 101000046,USA).

Western blot analysis

Cell or tissue samples were lysed in a lysis buffer with protease inhibitors. Subsequently, protein samples were separated by 10% SDS-PAGE and transferred onto nitrocellulose membranes. The membrane was blocked with 3% no-fat milk in PBST (PBS with 0.1% Tween 20) at 37°C for 1 h and incubated with the antibodies overnight at 4°C, and then with HRP goat anti-mouse IgG (H + L) or HRP goat anti-rabbit IgG (H + L) secondary antibody for 1 h at 37°C. Blot visualization was performed according to the manufacturer's instructions by using a Fully Automatic Chemiluminescence Image Analysis System. The antibody resources are as follows: GAPDH (Proteintech, 60004-1-Ig, China), β-Tubulin (Proteintech, 66240-1-Ig, China), P21 (Proteintech, 10355-1-AP, China), P16 (SANTA, sc-1661, USA), COL I (Proteintech, 66761-1-Ig, China), COL III (Proteintech, 22734-1-AP, China), MBNL2 (SANTA, sc-136167, USA), α-SMA (Abcam, ab124964, Great Britain), T-SMAD3 (Affinity Biosciences, AF6362, China), P-SMAD3 (Affinity Biosciences, AF3362, China), TGF-β1 (Abcam, ab215715, Great Britain), SENP1 (Proteintech, 25349-1-AP, China), KLF4 (Proteintech, 11880-1-AP, China), SUMO1 (Proteintech, 10329-1-AP, China), Anti-SUMO1/2/3 (PTM BIO, PTM-1109, China), POSTN (ABclonal Technology Co., Ltd., A14556, China).

Real-time PCR (RT-PCR)

The samples were lysed using the TRIzol reagent (Haigene, B0201, China), and the concentration and integrity of RNA samples were detected with the Nanodrop 2000 spectrophotometer (Thermo Scientific, USA). The volume of total RNA required for reverse transcription was calculated, and the first-strand cDNA was synthesized according to the instructions of the FastKing RT Kit (With gDNase). The cDNA was synthesized with 1 μg of total RNA following a Reverse transcription kit (Yeasen, 11141ES60, China). RT-PCR was processed by the SYBR Green Mix (Yeasen, 11184ES08, China) and detected the mRNA expression by the SLAN-96S system (SLAN, China). The data were analyzed using the $2^{-\Delta\Delta CT}$ method to quantify relative gene expression. The primers are as follows:

GAPDH-F: 5′-ACTCCCATTCTTCCACCTTTG-3′;
GAPDH-R: 5′-CCCTGTTGCTGTAGCCATATT-3′;
P16-F: 5′-CCGATACAGGTGAT GATGATGG-3′;
P16-R: 5′-CAGTACTACCAGAGTGTCTAGGA-3′;
P21-F: 5′-GCACTCTGAAGATGTGCCTATG-3′;
P21-R: 5′-CCCATAACTCCTTGCTAAC TCC-3′;
MBNL2-F: 5′-ACCACACCTGTCATTGTTCC-3′;
MBNL2-R: 5′-CCCTGC ATACCTCCAGTTTATC-3′;
COL I-F: 5′-CTGACGCATGGCCAAGAAGA-3′;
COL I-R: 5′-GTGCCATTGTGGCAGATACAG-3′;
COL III-F: 5′-CTGAACTCAAGAGCG GAGAATAC-3′;
COL III-R: 5′-CAGTCATGGGACTGGCATTTA-3′;
TGF-β1-F: 5′-CTGAACCAAGGAGACGGAATAC-3′;
TGF-β1-R: 5′- GTTTGGGACTGATCCC ATTGA-3′;
POSTN-F: 5′-TAAGTTCGTTCGTGGCAGCA-3′;
POSTN-R: 5′-AGGCTGAAGACTGCCTTGAAT-3′.

Immunofluorescence assay

Wash samples two times with PBS. Fix samples with 4% paraformaldehyde in PBS for 15 min at room temperature. Permeabilize samples with 0.1% Triton x-100 in PBS for 10 min. Incubate samples in 10% normal goat serum in PBS for 30 min at room temperature. Samples were stained with α-SMA (Abcam, ab124964, Great Britain), COL I (Proteintech, 66761-1-Ig, China), MBNL2(Santa Cruz, sc-136167, USA), and Vimentin (Proteintech, 10366-1-AP, China) antibody for 12 h. Then, the secondary antibody Alexa Fluor 488 or 647-labeled Goat Anti-Rabbit or Mouse IgG(H + L), was added for 1 h. DAPI was added for 5 min. Immunofluorescence was detected by microscope (Carl Zeiss, USA).

Collagen gel contraction assays

Harvest cells and resuspend in the desired medium. Prepare the collagen lattice by mixing 1 part of cell suspension and 4 parts of cold Collagen Gel Working Solution of Cell Contraction Assays (Cell Biolabs, BA-201, USA). Add 0.5 mL of the cell-collagen mixture per well in

a 24-well plate, and incubate for 1 h at 37°C. After collagen polymerization, 1 mL of culture medium is added atop each collagen gel lattice. The collagen gel size change (contraction index) can be measured at various times with a ruler or quantified with ImageJ software.

Co-immunoprecipitation (Co-IP)

Total cell lysates were prepared using NP40 lysis buffer with a freshly added protease inhibitor cocktail. The supernatants of cell lysates were obtained with centrifuging at 15,000 rpm at 4°C for 15 min, incubated with KLF4 polyclonal antibody (Proteintech, 11880-1-AP, China) overnight at 4°C. Then, 30 μL Protein A/G Magnetic Beads (MedChemExpress, HY-K0202, USA) were added to the samples at 4°C for 2 h. Co-IP proteins were eluted from the magnetic beads and immunoblotted with antibodies against KLF4 or SUMO1.

QUANTIFICATION AND STATISTICAL ANALYSIS

The statistical analyses were performed with GraphPad Prism 9.0 software (GraphPad Software, Inc, La Jolla, CA). Continuous variables were presented as the mean ± standard error of mean (SEM). Categorical variables were presented as numbers and percentages. Two-group comparisons were performed using Student's non-paired t-test. For comparisons among multiple groups, one-way ANOVA was used to compare the difference, respectively. Differences were considered statistically significant when $*p < 0.05$, $**p < 0.01$.